

Dip time-dependent SILAR synthesis and electrochemical study of highly flexible PPy-Cu(OH)₂ hybrid electrodes for supercapacitors

A. V. Thakur¹ · B. J. Lokhande¹

Received: 23 August 2016 / Revised: 24 October 2016 / Accepted: 31 December 2016 / Published online: 21 January 2017
© Springer-Verlag Berlin Heidelberg 2017

Abstract The effect of dip time variations on electrochemical performance of polypyrrole (PPy)-copper hydroxide hybrid thin-film electrodes was studied well in depth. Synthesis was carried out using a successive ionic layer adsorption and reaction (SILAR) method via an aqueous route, using 0.1 M pyrrole, 0.1 M Cu(NO₃)₂, and H₂O₂. The electrochemical analysis was made by using cyclic voltammetry (CV), galvanostatic charge-discharge (GCD) analysis, and electrochemical impedance spectroscopy (EIS). Scanning electron microscopy (SEM) image of optimized electrode shows nanolamellae-like structures. The characteristic peak observed in Fourier transform infrared (FTIR) analysis at 1558 cm⁻¹ validates the existence of PPy in hybrid electrode material, while the peaks observed at 21.5° and 44.5° in X-ray diffraction (XRD) patterns are evidence for triclinic Cu(OH)₂. The observed maximum values of specific capacitance (SC), specific power (SP), specific energy (SE), and coulombic efficiency (η) of the optimized electrode are 56.05 F/g, 10.48 Wh/kg, 11.11 kW/kg, and 46.47%, respectively. For originality and value, the SILAR synthesis of PPy-Cu(OH)₂ hybrid thin-film electrodes was carried out for the very first time. Synthesized electrodes showed improved surface structures and electrochemical stability than the pristine PPy electrodes which are necessary for the supercapacitive applications.

Keywords Polypyrrole · SILAR · Thin films · Electron microscopy · Supercapacitor

✉ B. J. Lokhande
bjlokhande@yahoo.com

¹ School of Physical Sciences, Solapur University, Solapur, M.S. 413 255, India

Introduction

Electrically conducting polymers (ECPs) are becoming very popular as they are applicable in various fields, viz. the artificial muscles and tissues [1], drug delivery system and biosensors [2, 3], gas sensors [4, 5], and optoelectronics [6–8]. Among all these applications, supercapacitors are gaining high attention [9]. In double-layer capacitors, the energy is stored in electrostatic way at the interface between a solid electrode and electrolyte, while in pseudocapacitors, it is stored in electrochemical way by either physisorption, intercalation-deintercalation, or redox reactions at a solid electrode surface at appropriate potential [10, 11]. ECPs have been investigated by the scientists for their use as electrode materials for supercapacitors. The ECPs are easy to produce, they have no constraints on the size, and they have the charge storage throughout the bulk volume. The conductivity of ECPs is due to the shifting of conjugate bonds [12, 13]. ECPs like polyaniline (PAni) [14], polythiophene (PTh) [15], and polyethylene dioxythiophene (PEDOT) have been extensively adopted as electrode materials for the supercapacitors. Polypyrrole (PPy) has few unique features, viz. low oxidation potential, water-soluble monomer, high charge storage ability, and good conductivity. Thus, PPy has been used as an electrode material for the supercapacitive electrode for energy and power applications [16]. Pure PPy thin-film electrodes showing highly porous morphology containing nanoparticles were reported by Shinde et al., exhibiting specific capacitance (SC) of 329 F/g in 0.5 M H₂SO₄ [17]. Shi and Zhitomirsky electrodeposited pristine PPy to exhibit a similar kind of morphology [18]. Metal oxides too have been used as electrode materials for pseudocapacitors [19–23]. Oxides and hydroxides of copper are being one of the best choices because of higher conductivity and multiple oxidation states of Cu [24]. Zhang et al. [25] and Dubal et al. [26] reported the synthesis of CuO

pseudocapacitor with flowerlike nanostructures, giving SC of 133.6 F/g in KOH. Lokhande et al. synthesized a thin film pseudocapacitive electrode of CuO multilayer nanosheets, showing SC of 43 F/g in Na₂SO₄ [27]. Wang et al. have grown CuO nanosheet arrays on nickel foam. The prepared faradaic electrode produced SC as high as 569 F/g in KOH [28]. Jadhav et al. prepared anodized copper hydroxide nanostructured electrode with SC of 230 F/g [29]. The inquisitiveness to observe the effect of hybridization of PPy with different metal oxides has forced the researchers throughout the universe to try different combinations of PPy and metal oxides [30–34]. The hydroxide phase of metal gives more specific capacitance than oxide. The incorporation CuO into the matrix of PPy was attempted for enhanced stability, high electrical conductivity, and superior electrochemical performance. Yin et al. synthesized the CuO/PPy 1D core-shell nanohybrids as an anode for lithium-ion batteries by a wire template method showing the initial capacity 991 mAh/g [31]. Zang et al. reported the facile synthesis of PPy coated nanowires [32]. A similar type of morphology was developed by Periasamy et al. to study glucose-oxidase and Horseradish peroxidase like activities of CuO/PPy [33]. Ates et al. have coated PPy/CuO on the carbon fiber micro-electrodes by chrono-amperometry to synthesize supercapacitive electrodes. These electrodes produced SC of 20 F/g at 5 mV/s in 0.5 M H₂SO₄ in the potential window of 0–0.8 V [34]. A successive ionic layer adsorption and reaction (SILAR) method was preferred over all the other methods of thin film deposition like chemical bath deposition [17], chemical vapor deposition and electrodeposition [35], spray pyrolysis [36, 37], sol-gel and spin coating. The advantages of SILAR over the other methods are as follows: (i) it put no constraints on the size of strips; (ii) it does not need any special mechanical arrangements like vacuum, temperature management, and spray unit; and (iii) it does not cause evolution of any poisonous gases by heating; hence, it is eco-friendly.

To the best of our literature survey, there is no work carried on SILAR synthesis of PPy-Cu(OH)₂ nanohybrids in addition to their electrochemical study by cyclic voltammetry (CV), chronopotentiometry (CP), and electrochemical impedance spectroscopy (EIS). Thus, the present research work aims to grow the PPy-Cu(OH)₂ hybrid thin films on stainless steel (SS) strips by a SILAR technique without using any binder. It was interesting to see the effect of dip time on their electrochemical behavior.

Experimental

Precursors

All the chemicals used for synthesis were of analytical grade, which were used without any further purification. Extra-pure

pyrrole and H₂SO₄ were purchased from Sigma-Aldrich while Cu(NO₃)₂ and H₂O₂ (30 wt%) were purchased from SD Fine Chemicals. H₂O₂ was used as an oxidizer without dilution. All the solutions were prepared in double-distilled water as a solvent.

Electrode preparation

In this binder-free electrode preparation, thin SS strips of 304 grade (size 1 × 5 cm²) were used as a conducting substrate. To get the rough finish, all the SS strips were mirror polished using a silicon carbide polish paper (grade 600). Then, these strips were ultrasonically cleaned for 20 min in double-distilled water at 310 K temperature. As reported in the literature, PPy material adheres more to the stainless steel treated with the nitric acid [28]; hence, these SS strips were thereafter treated with the dilute HNO₃ solution.

In the actual process, SS strips were first immersed in 0.1 M pyrrole (Py) dissolved in 0.5 M H₂SO₄ for variable time periods (5 to 20 s), where the polaron cations were adsorbed on the surface of SS strips. Then, these strips were immersed in 30 wt% H₂O₂ bath for 30 s. The process was continued by immersion of strips in 0.1 M of Cu(NO₃)₂ solution prepared using 0.5 M H₂SO₄ for different time periods (40 to 55 s), which was followed by the immersion of these strips in H₂O₂ bath again. In order to get uniform coating of electrode material on the strip surface, these strips were washed vigorously and pressure cleaned by the jets of double-distilled water to remove loosely bounded species from the electrode material. This completes one SILAR deposition cycle. One hundred twenty such SILAR deposition cycles were carried out. The dip time of 30 s was the same for each H₂O₂ bath. Electrodes prepared with different dip times in pyrrole, and the Cu(NO₃)₂ solutions as (5, 55), (10, 50), (15, 45), and (20, 40) for 120 SILAR cycles were denoted as N₁, N₂, N₃, and N₄, respectively (Table 1).

Characterizations

Structural analysis was carried out using an X-ray diffractometer (Ultima IV Rigaku D/max 2550Vb +18 kw with CuKα, λ = 1.54056 Å) in the range of diffraction angle (2θ) 10°–90°. An FTIR spectrophotometer (Nicolet iS 10, Thermo Scientific, USA) was used to verify the formation of polypyrrole. A scanning electron microscope (SEM S4300, Hitachi, Japan) was used to check the surface morphology. The weight of the deposited material was measured by a weight difference method using a high-accuracy analytical microbalance (Tapson-100TS, USA) of 10⁻² mg. Electrochemical characterizations were carried out using an electrochemical analyzer

Table 1 Sample codes with dip times and cycles for electrodes prepared using pyrrole and CuNO₃ and their SC values at 50 mV/s

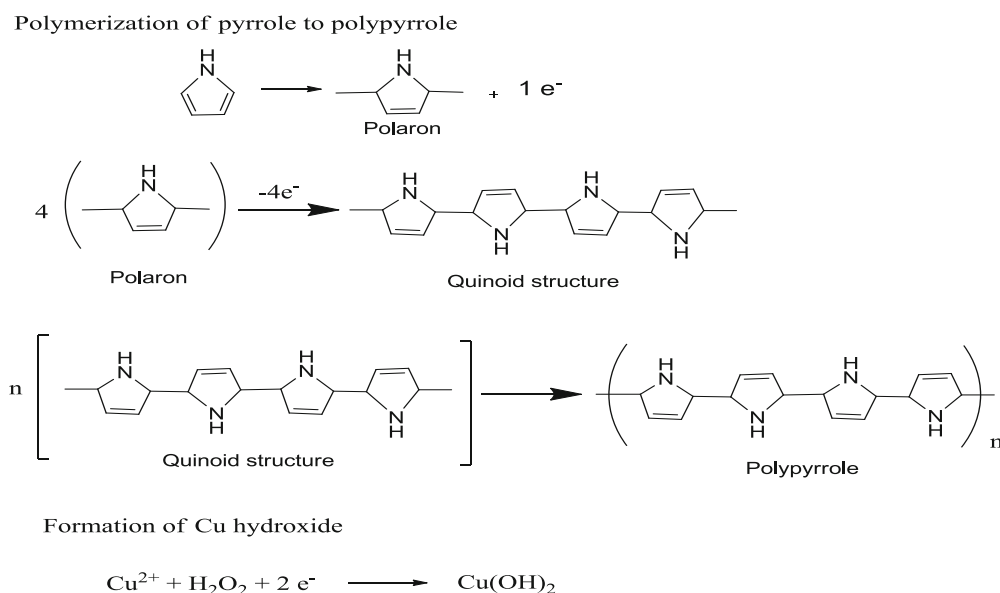
Electrode codes	Dip time in 0.1 M pyrrole, D_{t1} (s)	Dip time in H ₂ O ₂ (s)	Dip time in 0.1 M CuNO ₃ , D_{t2} (s)	Dip time in H ₂ O ₂ (s)	Dip cycles, D_c	Specific capacitance (SC) (F/g)
N ₁	05	30	55	30	120	35.51
N ₂	10	30	50	30	120	42.00
N ₃	15	30	45	30	120	45.02
N ₄	20	30	40	30	120	56.05

(CHI 408C, USA) with the standard three-electrode cell in which the prepared electrode acts as a working electrode and the platinum wire as a counter electrode while the saturated Ag/AgCl as a reference electrode. Electrochemical supercapacitive measurements were made using the data obtained from CV for the nearly 1 cm² surface area of the deposited material. The scan rate variations were applied to all electrodes within the potential window of -0.5 to 0.7 V in 0.5 M H₂SO₄. CV curves were used to calculate the SC using Eqs. 1 and 2 given in the text. Further, the charge-discharge behaviors of the electrodes were also studied at different current densities of 0.2 to 1 mA/cm² using CP. Chronopotentiometric parameters were calculated using the Eqs. 3, 4, 5, and 6. The EIS was also carried out to find R_s , R_{ct} , and R_w .

Results and discussion

Film formation mechanism

Pyrrole loses one electron in acidic medium and creates polaron. Polarons come together and form a bipolaron, trimer, quinoid structure, and finally, polypyrrole chain. Two electrons lost during the formation of polarons are taken by the H₂O₂ to form two OH⁻ ions. Cu²⁺ ions adsorbed on the strip combine with these hydroxyl ions to form the Cu(OH)₂. As the film grows layer by layer synchronously, the Cu(OH)₂ goes into the polymer matrix and forms the uniform hybrid PPy-Cu(OH)₂. The block schematics of SILAR showing a plausible nucleation and growth mechanism are shown in Fig. 1. The possible reactions during the film formation mechanism are shown below.

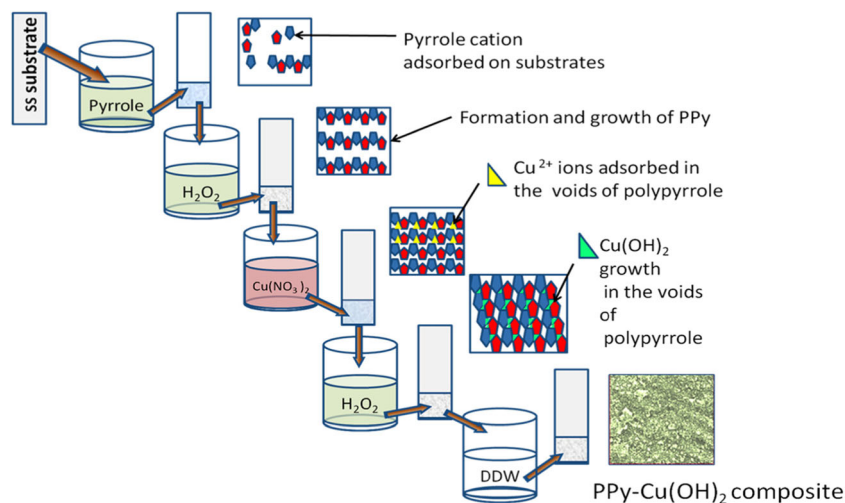


Physical characterization

The XRD patterns of electrode N₄ shows mostly amorphous nature with small peaks of monoclinic Cu(OH)₂ at the diffraction angles 21.503° and 44.5° (Fig. 2). The observed d values (interplanar spacing) are closely matching to the standard d values given in the JCPDS card no. 42-0638 (Table 2). The peaks

marked with asterisks are of SS strip as per the JCPDS card no. 35-1375. The XRD pattern of N₄ after CV analysis shows that peaks at 21.2° and 26.62° are closely matching to the standard data values in JCPDS card no. 72-1248, indicating the formation of orthorhombic CuSO₄, while the formation of monoclinic CuSO is confirmed by the peak observed at 31.53° matching to the standard data values in JCPDS card no. 76-0754.

Fig. 1 Block schematics of SILAR and (plausible) nucleation and growth



The FTIR spectrophotograph of electrode N_4 (Fig. 3) shows the peaks at wavenumbers 1570 cm^{-1} corresponding to C–C and C=C skeletal (ring) vibrations and 1658 cm^{-1} due to the C=C stretching; the peak at 1091 cm^{-1} is due to the C–H deformation vibration, peaks at 1140 and 1354 cm^{-1} are due to the C–N stretching, the peak at 796 cm^{-1} is due to the N–H wagging, and peaks at 2970 and 3186 cm^{-1} are due to the N–H stretching and vibrations. The peak at 3307 cm^{-1} is due to the =C–H stretching. All these peaks confirm the existence of PPy in the deposited material of electrode N_4 .

The scanning electron microscopy image of N_4 shows (Fig. 4a) the nanoclusters and nanolamellae observed for electrode N_4 . This morphology is different from the pristine PPy [10, 11], and this may be the reason for the improved electrochemical stability of the electrode. The elemental energy-dispersive X-ray (EDX) spectrum of the N_4 electrode shows the existence of C, N, O, and Cu which is one more evidence to the formation of the composite (Fig. 4b).

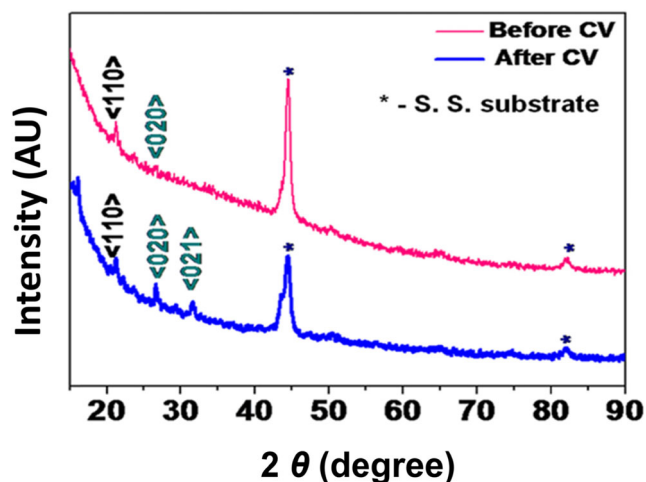


Fig. 2 XRD patterns of the N_4 electrode before and after CV analysis

Electrochemical characterization

Cyclic voltammetry

To study the capacitive behavior, all the electrodes N_1 , N_2 , N_3 , and N_4 were scanned at 5 mV/s in $0.5\text{ M H}_2\text{SO}_4$ within a potential window of -0.7 to 0.5 V (Fig. 5a). It was observed that the current integral increases with an increase in the dip time in pyrrole bath. The values of capacitance (C) and SC for different electrodes were calculated by using the following equations.

$$\text{Capacitance } (C) = \frac{\int_{v_1}^{v_2} I dv}{V \frac{dV}{dt}} \quad (1)$$

$$\text{Specific capacitance } (SC) \frac{C}{w} = \frac{\int_{v_1}^{v_2} I dv}{w(V) \frac{dV}{dt}} \quad (2)$$

where I is the average current in the redox cycle, V is the potential window, dv/dt is the voltage scan rate, C is the capacitance, and w is the mass of the active material dipped in the electrolyte.

Electrode N_4 shows the maximum SC of 56.054 F/g at 50 mV/s in $0.5\text{ M H}_2\text{SO}_4$. The values of SC for these electrodes are mentioned in Table 1. The variations of SC with the variations in the potential scan rate for electrode N_4 were studied (Fig. 5b). Values of SC at different scan rates were tabulated in the inset table of Fig. 5b. The electrode showed a nearly symmetric behavior on reduction and oxidation sweeps at lower scan rates. With an increase in the scan rate, the broad peaks on the oxidation curve went on increasing and the behavior became asymmetric. It was observed that as the scan rate increases, the current integral increases but SC decreases. The increase in current integral was not proportionate because the rate of doping and dedoping as well as the number of faradaic interactions did not increase in expected proportion with an increase in the scan rate.

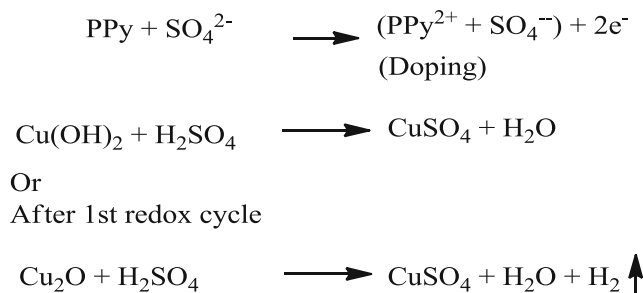
Table 2 XRD details for the N₄ electrode prepared using 0.1 M pyrrole and 0.1 M Cu(NO₃)₃ at dip times 20 and 40 s

Electrodes	Std. 2θ (°)	Observed 2θ (°)	Std. d (Å)	Observed d (Å)	h	k	l	JCPDS card no.
N ₄ before CV	21.50	21.26	4.1290	4.1757	1	1	0	42-0638
	44.50	44.52	2.0343	2.0330	1	2	2	
N ₄ after CV	21.27	21.20	4.1859	4.1757	2	0	0	72-1248
	26.51	26.62	3.3450	3.3450	0	2	0	
	31.51	31.53	2.8347	2.8347	0	2	1	

Plausible cell reactions during the CV analysis

During the oxidation sweep

Reactions at cathode

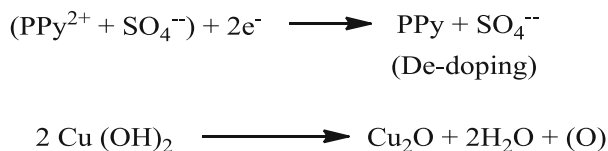


Reactions at anode

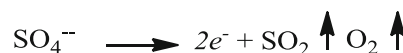


During the reduction sweep

Reactions at cathode



Reactions at anode



CV shows two sweeps, viz. oxidation and reduction. During the oxidation sweep, doping of PPy with the counter anion SO₄²⁻ took place. For reactions of Cu species, there are two cases which might have occurred.

- Case 1: The Cu(OH)₂ was converted into CuSO₄.
- Case 2: The Cu₂O formed during the reduction phase may have reacted with the sulfuric acid to give CuSO₄. In case 2, the oxidation of Cu⁺¹ to Cu²⁺ took place. Case 2 has less probability.

During the reduction sweep, the dedoping of anions from the PPy matrix took place while the Cu²⁺ cations that formed the Cu(OH)₂ get reduced to Cu⁺, forming Cu₂O. The redox reactions during the CV were found to

be irreversible. It may be due to the fact that the conversion of Cu₂O to CuSO₄ is an irreversible one. Hence, one could not find the broad peak at the reduction side of the CV plot.

Chronopotentiometry

The charge-discharge study of the N₄ electrode for different current densities was carried within the potential limits 0.7 to 0.4 V in 0.5 M H₂SO₄ (Fig. 5c). Various parameters were calculated using the following equations:

$$\text{Specific capacitance (SC)} = \frac{I_d \times t_d}{V_w} \tag{3}$$

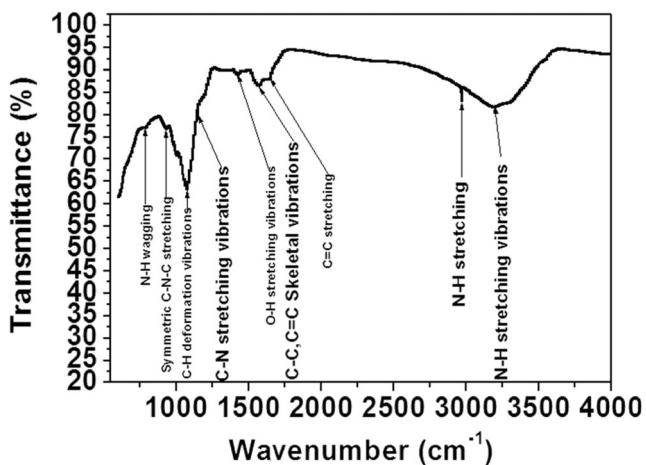


Fig. 3 FTIR spectroscopic pattern of the N_4 electrode

$$\text{Specific energy (SE)} = \frac{V \times I_d \times t_d}{w} \quad (4)$$

$$\text{Specific power (SP)} = \frac{V \times I_d}{w} \quad (5)$$

$$\text{Coulombic efficiency } (\eta) = \frac{t_d}{t_c} \times 100 \quad (6)$$

where V is the voltage; I_d and t_d are the discharging current and time, respectively; w is the weight of active electrode; and t_c is the charging time. For the N_4 electrode, the discharging profile showed fast discharging, indicating its suitability to the pulse power applications. The fast discharging denotes the dominance of pseudocapacitive nature. This was due to the increased amount of $\text{Cu}(\text{OH})_2$ in the electrode material. The specific capacitance was found to decrease with an increase in the current densities. The maximum observed value of

specific capacitance for N_4 electrodes was 78.10 F/g at 0.2 mA/cm^2 . The values of different chronopotentiometric parameters like SC, SE, SP, and η for N_4 are mentioned in Table 3.

EIS study

Electrochemical impedance spectroscopy of electrode N_4 was carried out in $0.5 \text{ M H}_2\text{SO}_4$ within the frequency ranges of 1 mHz to 100 kHz (Fig. 5d). The Nyquist plot consists of low frequency and high frequency regions. The solution resistance (R_s)/equivalent series resistance (ESR), low frequency region resistance (R_{low}), ionic resistance (R_i), charge transfer resistance (R_{ct}), and Warburg impedance (R_W) were evaluated from the Nyquist plot of the optimized electrode N_4 . The observed values of R_s , R_{low} , R_{ion} , R_{ct} , and R_W are 0.78 , 0.85 , 0.23 , 1 , and 1.23Ω , respectively. The inclination of the curve with the real axis was found to be $51^\circ 30'$. Two independent processes are responsible for the nature of the Nyquist plot. One is faradaic charge storage due to redox reactions while the other is diffusion of electrolyte ions which is represented by the Warburg element (W). The first process is the combined effect of charge transfer resistance (R_{ct}) and constant phase element (CPE). The non-uniform distribution of charges at an electrode surface gave rise to CPE; hence, the complete semicircle due to the parallel combination is not observed [29]. The reduction in R_{ct} of the composite electrode to an infinitesimal value as compared to that of the pristine PPy [30] is remarkable. It is most important for the power applications because of quick discharge.

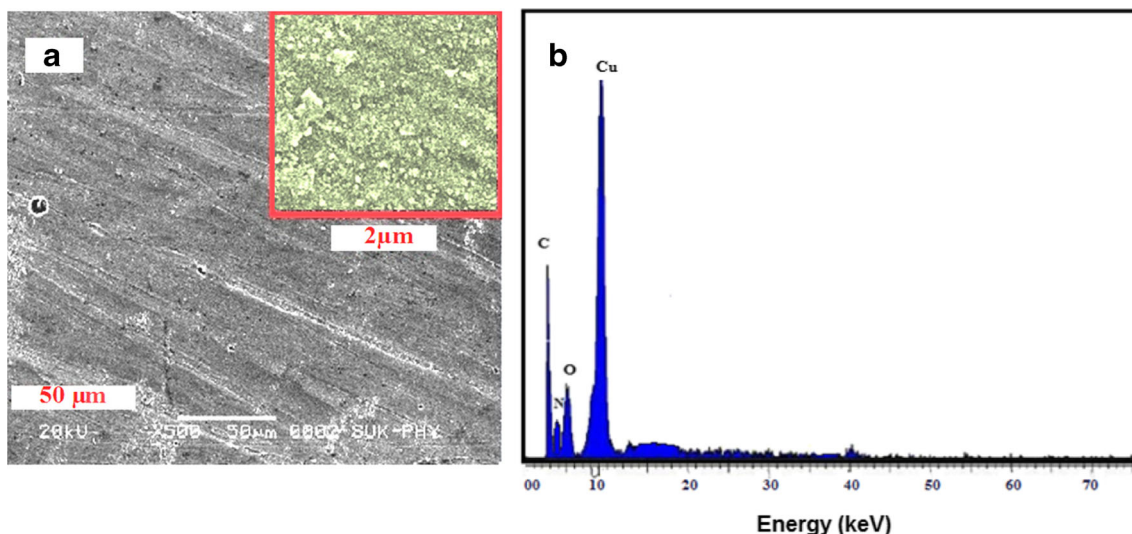


Fig. 4 a Nanoclusters and nanolamellae observed in the SEM picture of electrode N_4 . b EDX pattern of electrode N_4

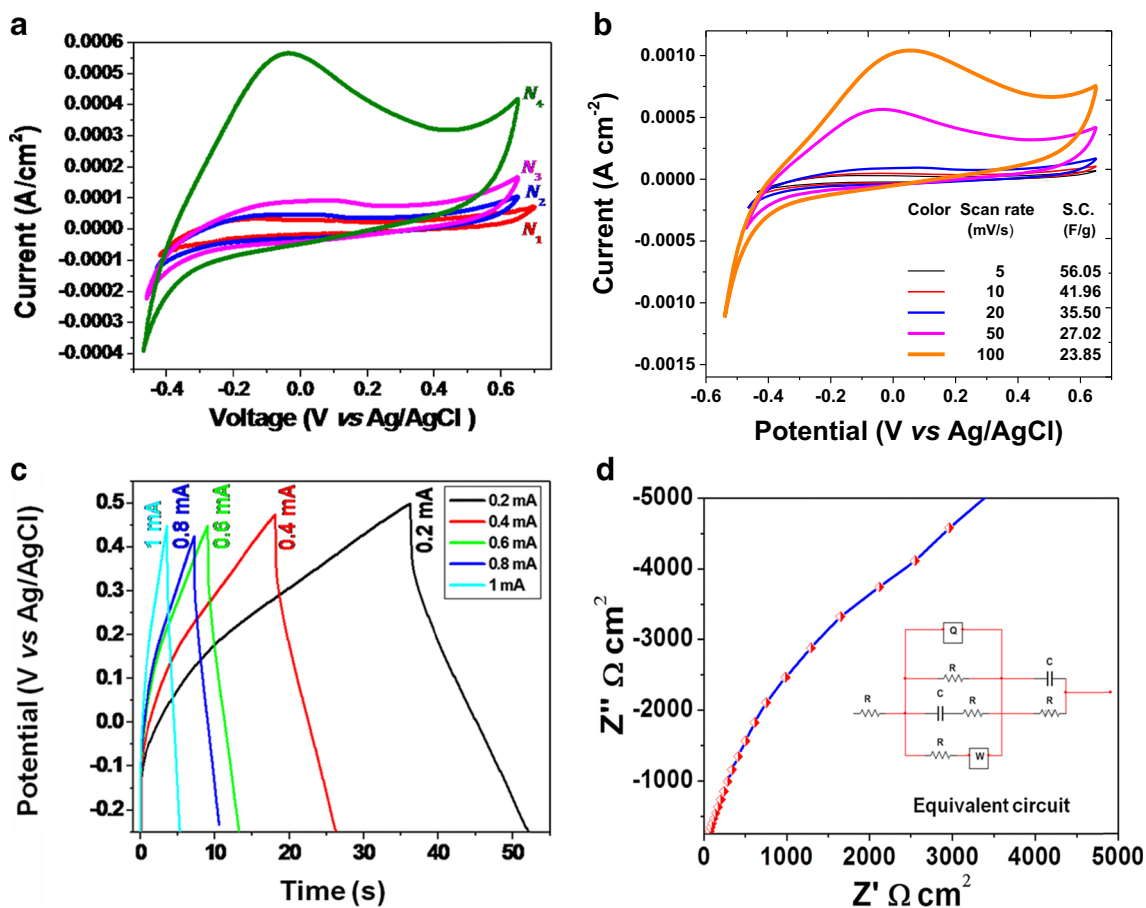


Fig. 5 a CV curves of all electrodes prepared at different dip times. b CV curves of electrode N₄ at different scan rates. c Charge-discharge curves of electrode N₄ at different current densities. d Nyquist plot and equivalent circuit for electrode N₄

Conclusion

Binder-free growth of PPy-Cu(OH)₂ nanohybrids on the stainless steel (SS) strips by SILAR deposition is possible. This synthesis shows the novel approach of growing PPy as well as Cu(OH)₂ in unison unlike the traditional ways in which the metal oxides/hydroxides were added in monomers during their polymerization. The prepared electrode material exhibits partly crystalline and partly amorphous nature due to the existence of triclinic Cu(OH)₂ in the hybrid. FTIR

spectrophotograph confirms the existence of PPy in the hybrid. Mixed capacitive behavior is observed due to the presence of faradaic charge storage in the bulk as well as redox reaction at the electrode electrolyte interface. The observed maximum values of specific capacitance (SC), specific power (SP), specific energy (SE), and coulombic efficiency (η) of the optimized electrode are 56.05 F/g, 10.48 Wh/kg, 11.11 kW/kg, and 46.47%, respectively. The electrode has relatively fast discharging, indicating its eligibility for power applications.

Table 3 Different chronopotentiometric parameters for the N₄ electrode

Electrodes	Current density (I_d), mA/cm ²	Specific capacitance (SC), F/g	Specific energy (SE), Wh/kg	Specific power (SP), kW/kg	η (%)
N ₄	0.2	78.10	10.57	2.22	46.47
	0.4	77.00	10.41	4.44	46.98
	0.6	68.23	9.92	6.66	47.71
	0.8	62.22	8.46	8.88	47.63
	1.0	34.90	4.75	11.11	42.07

Acknowledgements The authors are grateful to the DST-SERB for providing the electrochemical characterization.

References

1. Ateh DD, Navsaria HA, Vadgama P, (2006) *J R Soc Interf* 3:741–752
2. Vidal JC, Garcia E, Castillo JR, (1999) *Analyt Chim Acta* 385:213–222
3. Campbell TE, Hodgson AJ, Wallace GG, (1999) *Electroanalysis* 11:215–222
4. Kincal D, Kamer A, Child AD, Reynold JR, (1998) *Synthet Metal* 92:53–55
5. Kemp NT, Flanagan GU, Kaiser AB, Trodahl HJ, Chapman B, Partridge AC, Buckley RG, (1999) *Synthet Metal* 101:434–435
6. Stejskal J, Gilber RG, (2002) *Pure Appl Chem* 74:857–867
7. Saini P, Choudhary V, Singh BP, Mathur RB, Dhawan SK, (2009) *Mter Chem Phys* 113:919–926
8. Jang MS, Song S, Shim HK, (2000) *i Polymer* 41:5675–5679
9. Conway BE (1999) *Electrochemical supercapacitors: scientific fundamentals and technological applications*. Kluwer-Plenum, New York
10. Dubal DP, Patil SV, Kim WB, Lokhande CD, (2011) *Mater Lett* 65: 2628–31
11. Dubal DP, Lee SH, Kim JG, Kim WB, Lokhande CD, (2012) *J Mater Chem* 22:3044–52
12. Rudge A, Davey J, Raistrick I, Gottesfeld (1994) *J Power Source* :47–89
13. Shoa T, Madden JD, Fok CE, MirfaKhari T, (2008) *Adv Sci Tech* 61:26
14. Wang H, Hao Q, Yang X, Lu L, Wang X, (2010) *Appl Mater Interf* 2:821
15. Ambade RB, Ambade SB, Shrestha NK, Nah YC, Han SH, Lee W, Lee SH, (2013) *Chem Commun* 49:2308–2310
16. Davies A, Audette P, Farrow B, Hassan F, Chen Z, Choi JY, Yu A, (2011) *J Phys Chem C* 115:17612–17620
17. Shinde S, Gund GS, Kumbhar VS, Patil BH, Lokhande CD, (2013) *Eur Polym J* 49:3734–3739
18. Shi C, Zhitomirsky I, (2010) *Nanoscale Res Lett* 5:518–523
19. Zang J, Bao SJ, Li CM, Bian H, Cui X, Bao Q, (2008) *J Phys Chem C* 112:14843–47
20. Sharma RK, Rastogi AC, Desu SB, (2008) *Electrochim Acta* 53: 7690–95
21. Zhou C, Zhang Y, Li Y, (2013) *Nano Lett* 13:2078–2085
22. Qu Q, Zhu Y, Gao X, Wu Y, (2012) *Adv Energy Mater* 2:950–955
23. Liu Y, Zhang B, Yang Y, Chang Z, Wen Z, Wu Y, (2013) *J Mater Chem A* 1:13582–87
24. Zhang H, Zhang M, (2008) *Mater Chem Phys* 108:184–187
25. Zhang H, Feng J, Zhang M, (2008) *Mater Res Bull* 43:3221–3
26. Dubal DP, Dhawale DS, Salunke RR, Jamadade VS, Lokhande CD, (2010) *J Alloy Compd* 492:26–30
27. Patake VD, Joshi SS, Lokhande CD, Joo OS, (2009) *Mater Chem Phys* 114:6–9
28. Wang G, Huang J, Chen S, Gao Y, Cao D, (2011) *J Power Source* 196:5756–5760
29. Jadhav VV, Shinde DV, Patil SA, Zate MK, Osta S, Osta A, Mane RS, Han SH, (2014) *J Nano Engineer Manufact* 4:1–5
30. Liew SY, Thielemans W, Walsh DA, (2010) *J Phys Chem C* 114: 17926–17933
31. Yin Z, Ding Y, Elsevier, (2012) *Electrochem Comm* 20:40–43
32. Liu Y, Liu Z, Lu N, Preiss E, Poyraz S, Kim MJ, Zhang X, (2012) *Chem Commun* 48:2621–2623
33. Periasamy AP, Roya P, Wua WP, Huanga YH, Chang HT, (2016) *Electrochim Acta* 215:253–260
34. Ates M, Serin MA, Ekmen I, Ertas YN, (2015) *Polym Bull* 72: 2573–2589. doi:10.1007/s00289-015-1422-4
35. Karaca E, Pekmez NO, Pekmez K, (2014) *Electrochim Acta* 147: 545–556
36. Lokhande BJ, Ambare RC, Mane RS, Bhardwaj SR, (2013) *Curr Appl Phys* 13:985–989
37. Lokhande BJ, Patil PS, Uplane MD, (2004) *Mater Chem Phys* 84: 238–242